Programmable mechanical metamaterials

Florijn, H.C.B.

CHAPTER 3

SOFT MECHANISM

The soft mechanism qualitatively describes the mechanics of the confined biholar sheet well, section 2.6. In this chapter we discuss the biholar mechanism in more detail and especially the different bifurcation scenarios that are responsible for the different mechanical regimes. We start with a one degree mechanism, section 3.1. Then we add horizontal and linear springs and calculate the energy for the control parameters ε_x and ε_y, and analyze the stability and bifurcations, section 3.2. Finally, a geometric interpretation of the four different mechanical regimes is presented in section 3.3, which can be used as a guideline to rationally design mechanical metamaterials with confinement controlled response.

3.1 Biholar Mechanism

To qualitatively understand the mechanics of confined biholar sheets, we note that when $t \to 0$, the material's low energy deformations are equivalent to that of a mechanism consisting of rigid rectangles connected by hinges at their corners, positioned in the center of the thinnest part of the filament between two neighboring holes (Fig. 3.1).

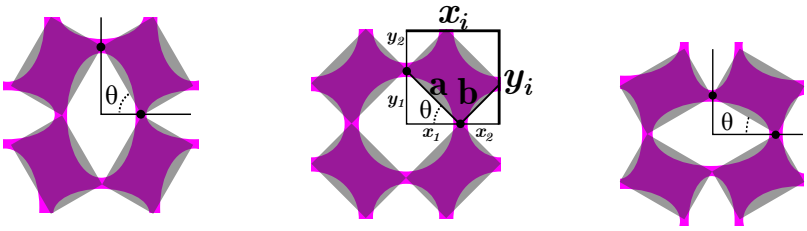

(a) $\theta > \pi/4$ (b) $\theta = \pi/4$ (c) $\theta < \pi/4$

FIGURE 3.1: Biholar Mechanism: A collection of rectangles connected with hinges (gray) represents the biholar sample (pink). The state of this mechanism is described by a single degree of freedom, θ, which determines the internal dimensions x_i and y_i. (a) For $\theta > \pi/4$, the mechanism is x-polarized. (b) For $\theta = \pi/4$ the system is in the undeformed configuration. (c) For $\theta < \pi/4$ the mechanism is y-polarized.

We define the dimensionless biholarity χ of the mechanism as:

$$\chi = \frac{2(|a-b|)}{a+b}, \tag{3.1}$$

where $a \geq b$ are the sides of the rectangles (Fig. 3.1b).
There is a one-to-one mapping between the definitions of biholarity for the mechanism and for the biholar sample. We can write

$$a = (r_1 + \frac{1}{2}t)\sqrt{2} \tag{3.2}$$

$$b = (r_2 + \frac{1}{2}t)\sqrt{2}, \tag{3.3}$$

where r_1 and r_2 are the radii of the big and small holes and t is the thickness of the most slender part of the filament between these holes. Substituting these equations into equation (3.1) we obtain

$$\chi = \frac{2|r_1 - r_2|}{p}, \tag{3.4}$$

which shows the consistency of the definitions of χ for the biholar samples the mechanism.
The state of this mechanism is described by a single degree of freedom, θ. To avoid self intersection of the mechanism, $0 \leq \theta \leq \pi/2$. This simple one-degree-of-freedom-mechanism captures the pattern transformation as observed in the biholar sample; for $\theta > \pi/4$, the mechanism is x-polarized (Fig. 3.1(a)) and for $\theta < \pi/4$ the mechanism is y-polarized (Fig. 3.1(c)).
The angle θ also determines the internal dimensions x_i and y_i:

$$x_i = x_1 + x_2 = a\cos(\theta) + b\sin(\theta) \tag{3.5}$$
$$y_i = y_1 + y_2 = a\sin(\theta) + b\cos(\theta) \tag{3.6}$$

For simplicity we will set $x_i(\pi/4) = y_i(\pi/4) = 1$, so that $a + b = \sqrt{2}$, equivalent to pitch $p = 1$. The biholarity is then given as $\chi = 2\frac{(a-b)}{a+b} = \sqrt{2}(a-b)$ and the allowed range of biholarity is $\chi \in [0, 2]$.

3.2 Energy, Stability and Bifurcations

To model the storing of elastic energy, we couple the biholar mechanism to the outside walls of a box, with dimensions $2x_o$ and $2y_o$, with a set of linear springs of rest length zero. The box models the lateral confinement and uniaxial compression.

The potential energy E in the system is written as:

$$E = 4 \cdot \frac{1}{2} k_x \delta l_x^2 + 4 \cdot \frac{1}{2} k_y \delta l_y^2 \tag{3.7}$$

where δl_x (δl_y) is the change in length of the horizontal (vertical) springs with respect to their rest length. As the rest length of the springs is zero,

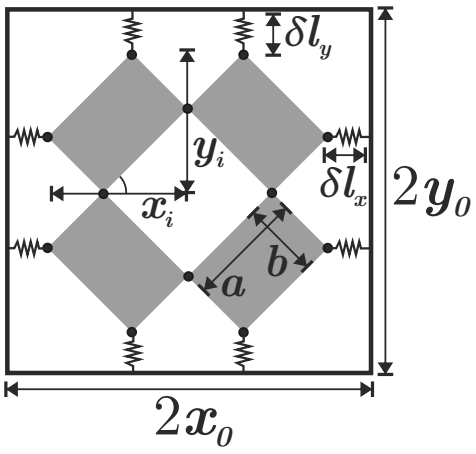

FIGURE 3.2: Soft Biholar Mechanism. The mechanism, with internal dimensions x_i and y_i, is placed inside a box, with dimensions $2x_o$ and $2y_o$, and connected to the box with linear springs, of lengths δl_x and δl_y.

the in length of the springs is simply given by the difference between the outside wall and the internal dimensions of the mechanism:

$$\delta l_x = x_o - x_i(\theta) \tag{3.8}$$
$$\delta l_y = y_o - y_i(\theta) \tag{3.9}$$

Similar to experiments, the control parameters ε_x and ε_y are used to deform the outside walls of the box, such that the dimensions of the box are $2x_o = 2 - 2\varepsilon_x$ and $2y_o = 2 - 2\varepsilon_y$. Now, also setting $k_x = k_y = 0.5$, the potential energy can be written as:

$$E = (1 - \varepsilon_x - x_i(\theta))^2 + (1 - \varepsilon_y - y_i(\theta))^2 \tag{3.10}$$

For each set of control parameters ε_x and ε_y there is an energy landscape as a function of θ for which we have to find the mechanical equilibrium[1],

[1]In the Appendix A Lagrange multipliers are used to directly find a (implicit) relation between the force ($F(\theta)$) and deformation (ε_y)

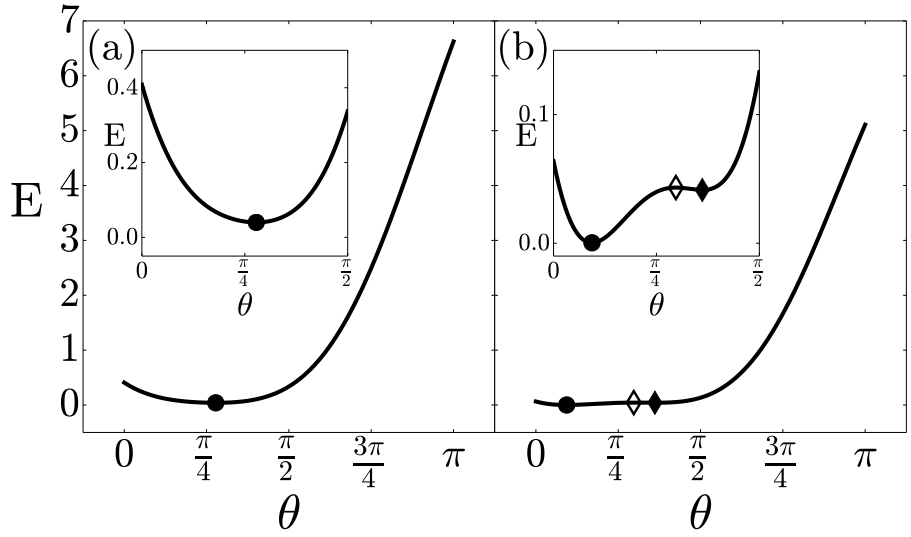

FIGURE 3.3: Potential energy as a function of internal degree of freedom θ. (a) For $\varepsilon_x = -0.03$ and $\varepsilon_y = -0.2$ the energy has one global minimum (black dot). (b) For $\varepsilon_x = -0.0355$ and $\varepsilon_y = 0.2$ the energy has three states of mechanical equilibrium, indicate by the black dot (abolute minimum), black diamond (local minimum) and open diamond (local maximum).

$dE/d\theta = 0$. The value of θ_{eq} at the equilibrium points will be the orientation of the biholar mechanism, with energy $E_{eq} = E(\theta_{eq})$.
Depending on the values of ε_x and ε_y, the energy landscape can have one or three stable states. Shown in Fig. 3.3 are two examples of the $E(\theta)$-curves for different values of the control parameters. In Fig. 3.3(a), $\varepsilon_x = -0.03$ and $\varepsilon_y = -0.2$ and the energy landscape has a single minimum, with one stable equilibrium, indicated by the black dot. For $\varepsilon_x = -0.0355$ and $\varepsilon_y = 0.2$ the potential energy obtains a bump, see Fig. refEnergyExamples(b), resulting in 3 states of mechanical equilibrium. Two of these states are stable, corresponding to the (local) minima (black dot for global minimum, full diamond for local minima), and one state is unstable, corresponding to a local maximum (open diamond).

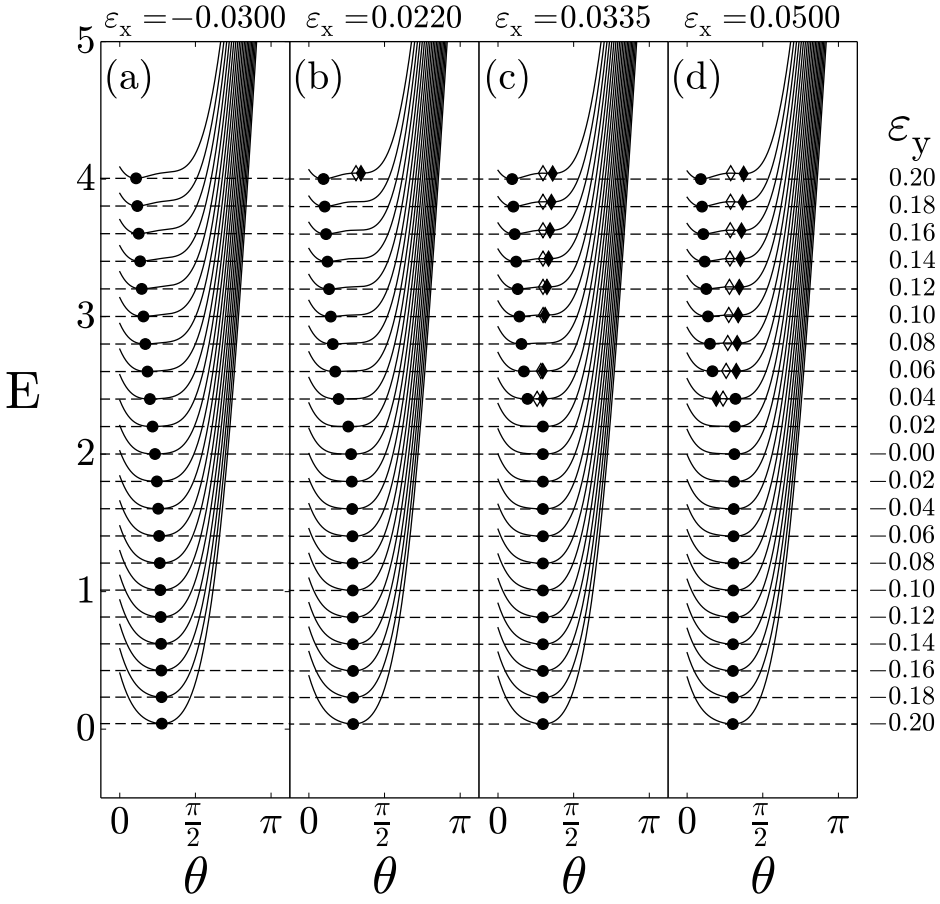

FIGURE 3.4: $E(\theta)$-curves for increasing ε_y and for four different, but fixed, values of ε_x; (a) $\varepsilon_x = -0.03$, (b) $\varepsilon_x = 0.022$, (c) $\varepsilon_x = 0.0355$ and (d) $\varepsilon_x = 0.05$. Global minima are indicated with an black dot, local minima with an black diamond, local maxima with an open diamond.

In the experiments, the horizontal confinement ε_x is fixed while ε_y is varied continuously. Presented in Fig. 3.4(a)-(d) are $E(\theta)$-curves for four different values of horizontal confinement, $\varepsilon_x = \{-0.03, 0.022, 0.0355, 0.05\}$, for a range of increasing ε_y. All curves are displayed with an offset for clarity.
In Fig. 3.4(a), $\varepsilon_x = -0.03$ and ε_y is continuously increased from -0.2 to 0.2. All curves have one global minimum that is shifting towards $\theta = 0$ for increasing vertical strain. For higher values of ε_y the onset of a bump is emerging in the energy landscape.
For $\varepsilon_x = 0.022$, Fig. 3.4(b), a similar behavior of the global minimum is observed, although the most significant change in the position of the local minimum gets concentrated between $0.02 < \varepsilon_y < 0.04$. Moreover, for $\varepsilon_y = 0.2$ a bump is visible in the $E(\theta)$-curve, resulting in a pair of equilibrium states, one stable (full diamond) and one unstable (open diamond). The creation, or annihilation, of two new equilibrium states is associated with a saddle-node bifurcation.
Increasing the horizontal confinement to $\varepsilon_x = 0.0355$, the energy initially has one minimum. However, for $\varepsilon_y = 0.04$, a pair of local minimum and maximum is appearing. Next, for $\varepsilon_y = 0.06$, two equilibrium states move towards each other and finally annihilate for $\varepsilon_y = 0.08$. Moreover, for $\varepsilon_y = 0.10$, another pair of equilibrium states is created and is still present for higher values of applied vertical strain.
Finally, increasing the horizontal confinement to $\varepsilon_x = 0.05$, results in similar $E(\theta)$-curves for small ε_y. However, as ε_y is increased, the location of the global minimum is shifting towards higher values of θ. At $\varepsilon_y = 0.04$ a pair of a local maximum and minimum is created to the left of the global minimum, whereas for $\varepsilon_y > 0.04$ this pair is created to the right of the global minimum.
As ε_y is increased from $\varepsilon_y = -0.2$ to $\varepsilon_y = 0.2$, the path followed by the mechanism, traced out by the equilibrium points of the energy, is different for distinct values of ε_x. Shown in figure 3.5 are the equilibrium points θ_{eq} ((a)-(d)) and E_{eq} ((e)-(h)) as a function of ε_y for the different values of ε_x. Presented in the last row of figure 3.5 are the corresponding forces directly computed using $F(\varepsilon_y) = -dE_{eq}/d\varepsilon_y$.

regime (*i*) In Fig. 3.5 (a) (page 52), for $\varepsilon_x = -0.03$, as the control parameter ε_y is increased from $\varepsilon_y = -0.2$ to $\varepsilon_y = 0.2$, the mechanism follows a single stable branch, indicated by A. The corresponding energy E_{eq} is single valued and is decreasing for $\varepsilon_y < 0$ and increasing for $\varepsilon_y > 0$, resulting in a monotonic force curve, that we classify as regime (*i*).

regime (*ii*) Shown in Fig. 3.5 (b), the mechanism follows a stable branch A for uniaxial compression. Only now, most of the change in θ_{eq} gets focused around $\varepsilon_y = 0.00$. Moreover, for high values of ε_y and θ_{eq}, a stable branch B (black) and an unstable branch C (dashed gray) appear through a saddle-node bifurcation. Since these new branches are not connected to branch A, the sample can not reach these states when subjected to a simple uniaxial deformation.
In Fig. 3.5 (f), around $\varepsilon_y = 0.00$, a bump is emerging in the energy curve, leading to a region of negative incremental stiffness in the accompanying force curve, Fig. 3.5 (j). Hence, the system is in regime (*ii*). Moreover, for high values of ε_y the energy and the force curves becomes multivalued due to branches B and C; a local minimum (black) and maximum (dashed gray) appear at high energies.

regime (*iii*) For $\varepsilon_x = 0.0335$, Fig. 3.5 (c), branch A has become S-shaped and is split into two stable branches, A (black) and A'' (gray), connected by an unstable branch A' (dashed gray), via two saddle-node-bifurcations. This entire branch exhibits hysteretic behavior and bistability. Monotonically increasing ε_y, starting from $\varepsilon_y = -0.2$, θ_{eq} jumps from the stable branch A to stable branch A'' at the location indicated by the black arrow. Monotonically decreasing the system from $\varepsilon_y = 0.2$ and low θ, we move along branch A'' and jump to branch A at a different value of ε_y. For all values of ε_y in the region enclosed by the two arrows there are two stable states, i.e. the system is bistable.
The energy for a biholar mechanisme in regime *iii*, Fig. 3.5(c) takes a more complicated shape and forms a loop around $\varepsilon_y = 0.1$, see inset, consisting of two segments of local minima connected by an unstable segment of local maxima. Depending on the path followed, the energy jumps from a high value to a low value at different locations, indicated by the gray and black arrow. Note that the energy jump from the black curve to the gray curve (compressing) is much higher than from gray to black (decompress-

ing).
The hysteretic region is also clearly present in the $F(\varepsilon_y)$-curve, Fig. 3.5 (k), as the force follows different paths for compression and decompression, indicated by the black and gray arrows. Note that branches B and C come close to the point where branch A and A' meet, and will eventually cross to form a transcritical bifurcation at the transition from regime *iii* to *iv* .

regime (*iv*) For $\varepsilon_x = 0.05$, Fig. 3.5 (d), we observe the outcome of a system that has moved away from the transcritical bifurcation. At the *iii*-*iv*-transition, stable branches A and B and unstable branches A' and C, as present in Fig. 3.5 (c), meet in one limit point, a transcritical bifurcation, and exchange stability. As ε_x is increased from $\varepsilon_{x_{iii-iv}}$, the value of ε_x at the *iii*-*iv*-transition, to $\varepsilon_x = 0.05$, branch A and B get connected and separated from the second branches A'' and $C + A'$. When ε_y is increased, starting from $\varepsilon_y = -0.2$, θ_{eq}, follows stable branch $A + B$ and, in contrast to Fig. 3.5 (a)-(c), is monotonically *increasing*. Hence, the system is in regime (*iv*).
The energy equilibria are split into two seperate curves, Fig. 3.5 (h), the black curve belonging to trajectory $A + B$ and a gray curve belonging two A'' and $C + A'$. Although these two distinct energy curves cross, see inset, the trajectories in θ_{eq} are separated and the system does not minimize its energy by jumping to a lower energy branch. The force, Fig. 3.5 (l), derived from E_{eq}, is monotonic again for monotonically increasing ε_y, starting from $\varepsilon_y < 0$.
As shown in Fig. 3.5, the soft biholar mechanism captures the phenomenology found in the experimental biholar sheets very well. Moreover, Fig. 3.5 (a)-(d) gives deep inside in the different bifurcation scenarios leading to the four different mechanical regimes.

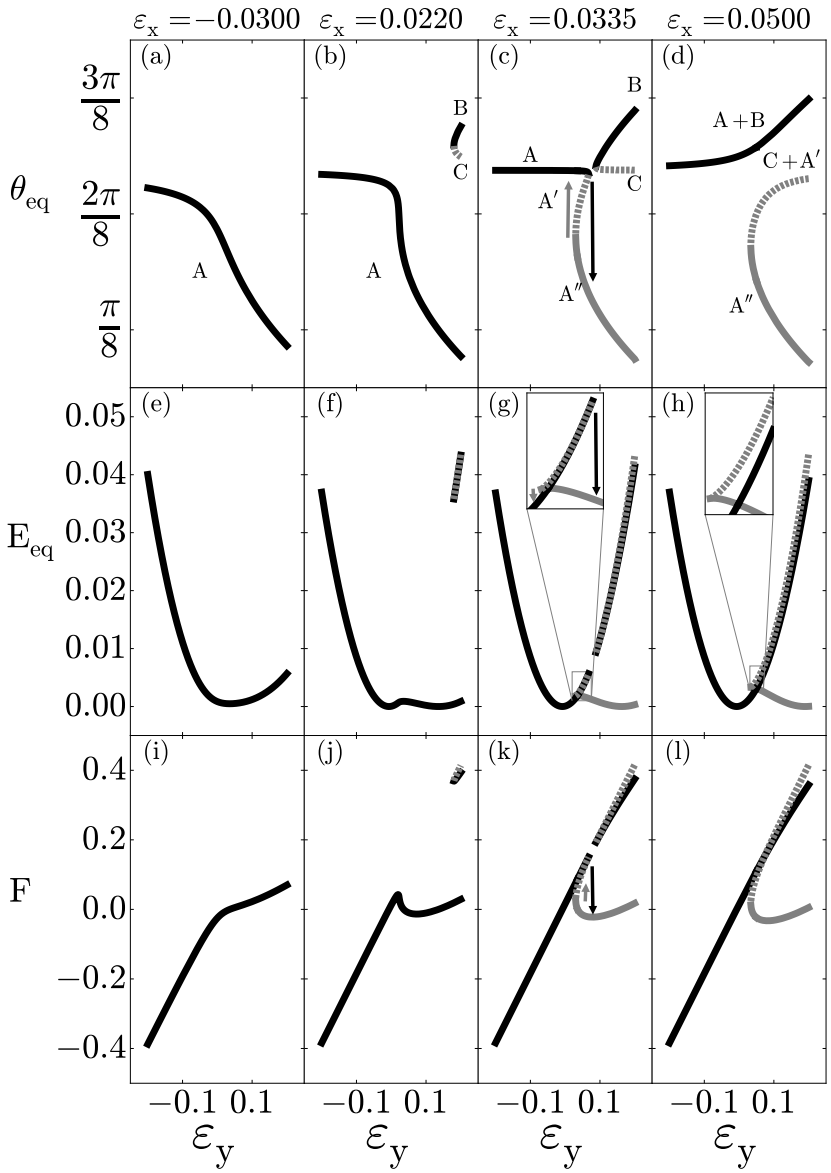

FIGURE 3.5: (a)-(d) Equilibrium angles as a function of uniaxial deformation ε_y, showing that the trajectories followed by the soft biholar mechanism in regimes *i-iv* (different values of ε_x). (e)-(h) Equilibrium energy as a function of ε_y. (i)-(l) Forces derived from equilibrium energies as function of ε_y (dashed for unstable states).

3.3 Geometrical Interpretation

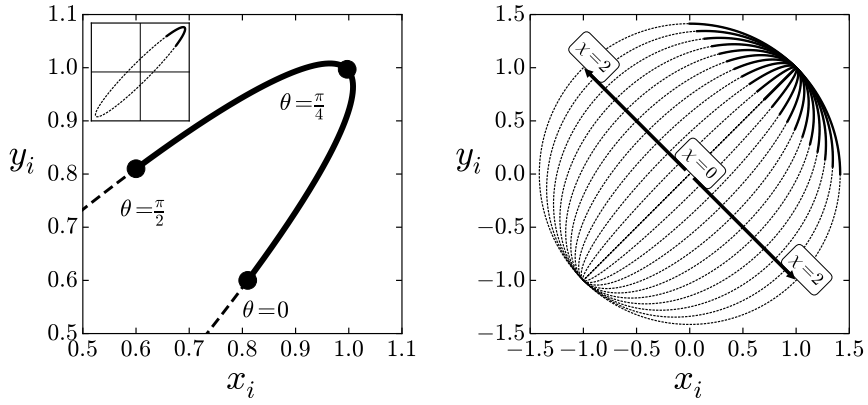

FIGURE 3.6: (a) The M-curve for a biholar mechanism, shown here for $\chi = 0.3$, is part of an ellipse, that is rotated by $\pi/4$ with respect to the origin. (b) M-curves for different values of χ with $a + b = \sqrt{2}$ and $\theta \in [0, \pi/2]$.

The internal dimension of the soft mechanism are given by equations 3.5 and 3.6. Now, using $(x_i + y_i)/(a + b) = \cos(\theta) + \sin(\theta)$ and $(x_i - y_i)/(a - b) = \cos(\theta) - \sin(\theta)$, these equations are rewritten to obtain:

$$\left(\frac{x_i + y_i}{2}\right)^2 + \left(\frac{x_i - y_i}{\chi}\right)^2 = 1 \tag{3.11}$$

So the relation between the internal dimensions y_i and x_i for a non-intersecting biholar mechanism, the *M-curve*, describes part of an ellipse (Fig. 3.6a) that is rotated by $\pi/4$ with respect to the origin. The major axis of the ellipse is fixed and given by $\sqrt{2}$ and the minor axis depends on biholarity and is given by $\chi/\sqrt{2}$. So, as we increase the biholarity, the minor axis of the ellipse will increase from zero to $\sqrt{2}$, see Fig. 3.6b.

A geometric interpretation of the various equilibria and their bifurcations, as ε_x and ε_y are varied, provides much insight. As illustrated in Fig. 3.6, the relation between the x_i and y_i can be represented as a smooth curve, which we refer to as M (for mechanism). For given dimensions of the

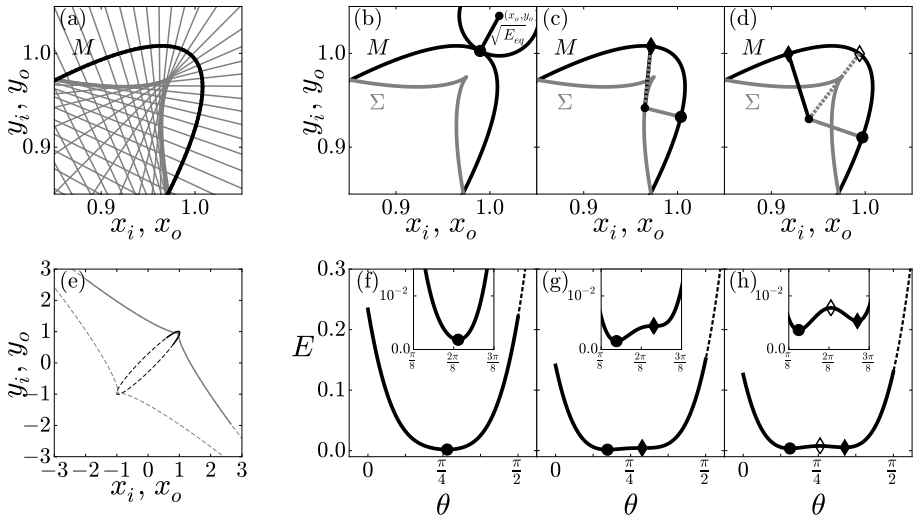

FIGURE 3.7: (a) The envelope of all curves normal to M mark the evolute Σ of M. (e) M-Curve and evolute, dashed lines indicate non-physical solutions where $\theta \notin \{0, \pi/2\}$. (b)-(d) Depending if (x_o, y_o) is outside, precisely at, or inside Σ, one, two or three vectors from (x_o, y_o) normal to M can be drawn. (f)-(h) The normal vectors are associated with the equilibria of the system. The length of the normal vectors gives the square root of the equilibrium energy, the intersection of the normal vector with M marks the equilibrium state θ_{eq} of the mechanism.

bounding box (x_o, y_o), the distance from (x_o, y_o) to M is

$$d = \sqrt{(x_o - x_i(\theta))^2 + (y_o - y_i(\theta))^2} = \sqrt{E(\theta)}, \tag{3.12}$$

for $k_x = k_y = 0.5$.
As extrema of $d = \sqrt{E(\theta)}$ are also extrema of $E(\theta)$, we can find equilibria of $E(\theta)$ by searching for points $(x_i(\theta_{eq}), y_i(\theta_{eq}))$ on M that minimize or maximize the distance d between (x_o, y_o) and M. This implies finding lines that are normal to M and intersect (x_o, y_o). In other words, stable (unstable) equilibria of E thus correspond to points $(x_i(\theta_{eq}), y_i(\theta_{eq}))$ on M, tangent to circles centered at (x_o, y_o) with radius $E^{1/2}$.
Shown in Fig. 3.7(a) are a selection of lines that are normal to M. The envelope of all curves normal to M mark the evolute Σ, the locus of all centers

of curvature of M. For a point (x_o, y_o) outside the evolute, one vector[2] of length $\sqrt{E_{eq}}$, normal to M can be drawn (Fig. 3.7(b)). As shown in figures 3.7(e) and (f), the intersection of the black normal vector with M corresponds to a state $(x_i(\theta_{eq}), y_i(\theta_{eq}))$ that is a global minimum (black dot) of d and therefore E.
For a point (x_o, y_o) exactly at Σ, two normal vectors can be drawn (Fig. 3.7(c). The intersection of the gray normal vector with M corresponds to a state $(x_i(\theta_{eq}), y_i(\theta_{eq}))$ that is a global minimum, see Fig. 3.7(g), while the intersection of black-gray dashed normal vector with M corresponds to a flat region in $E(\theta)$.
For a point (x_o, y_o) inside the evolute, three vectors normal to M can be drawn (Fig. 3.7(d)). The gray normal vector corresponds to a global minimum (black dot), the dashed gray normal vector to a local maximum (open diamond) and the black vector to a local minimum (black diamond). In summary, depending if (x_o, y_o) is outside, precisely at, or inside Σ, one, two or three vectors from (x_o, y_o) normal to M can be drawn. Each normal vector is associated with an equilibrium state of the soft mechanism, as it minimizes or maximizes the distance $d(\theta)$, and hence $E(\theta)$. The location of the intersection of the normal vector with M, gives the equilibrium state $(x_i(\theta_{eq}), y_i(\theta_{eq}))$, with equilibrium energy E_{eq}, the square of the length of the normal vector.

The experimental protocol varies y_o at fixed x_o. Hence, the experimental protocol follows vertical lines in the x_i-$y - i$-plots, see Fig. 3.8. We immediately see that, depending on the choice of x_o, these trajectories cross or do not cross M and Σ. Repeating the geometric construction as discussed above provides the corresponding stable and unstable equilibria along the trajectory. When the vertical lines crosses Σ, saddle-node bifurcations occur, as a pair of local maxima and minima emerges.
We now explore this model to understand the transition A from monotonic to non-monotonic force curves, the transition B that leads to hysteresis, and the transition C where the differently polarized branches become separated. In Fig. 3.8 we indicate the four trajectories corresponding to

[2]In general, depending if (x_o, y_o) is outside, at or inside Σ there are two, three or four vectors normal to an ellipse. However, since we restrict the M-curve to represent only physical states, $\theta \in [0, \pi/2]$, there are one, two or three vectors normal to M.

the four different mechanical regimes (*i*)-(*iv*), as well as three trajectories labeled *A*, *B* and *C* that correspond to marginal curves which separate scenarios *(i)-(iv)*.

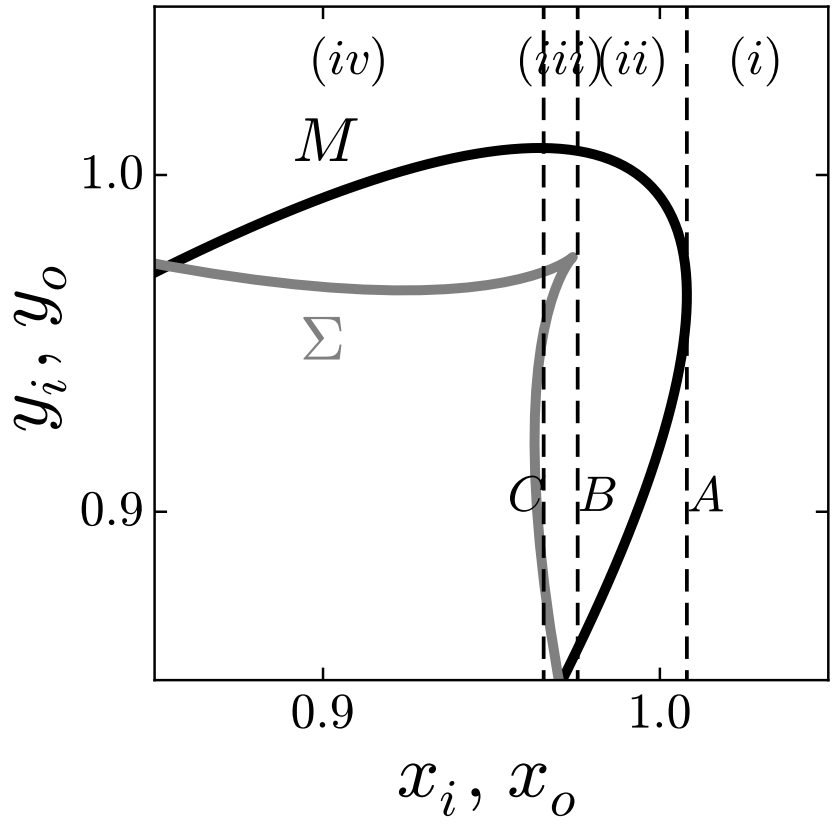

FIGURE 3.8: The experimental protocol, varying y_o while keeping x_o fixed, is visible as vertical lines in the x_i-y_i-plots. Depending on the choice of x_o, these trajectories cross or do not cross the M-curve and/or the Σ-curve, which identifies regime (*i*)-(*iv*). The marginal trajectories (*A*, *B* and *C*), are precisely located at the transitions between the regimes.

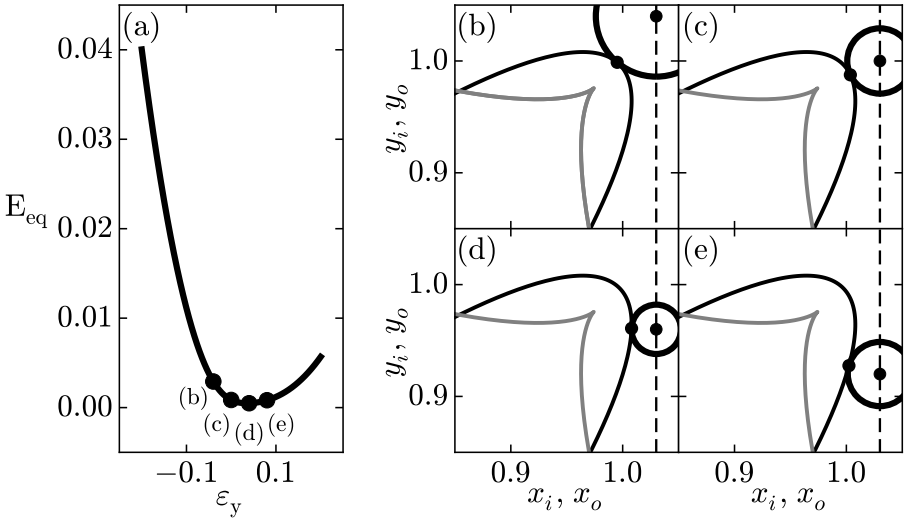

FIGURE 3.9: (a) Equilibrium energy of the vertical trajectory for a biholar mechanism with $\chi = 0.3$ and $x_o = 1.0300$ ($\varepsilon_x = -0.0300$). (b)-(e) Four different points at the trajectory with their corresponding equilibrium energy circles that are tangential to M. The equilibrium state $(x_o(\theta), y_o(\theta))$ is the point where the energy circle meets the M-curve (gray diamond).

Regime (i) The value of x_o is chosen such, $\varepsilon_y = 1 - x_o = -0.0300$, that the trajectory of y_o is outside of M and Σ, Fig. 3.9. Shown in Fig. 3.9(a) is the equilibrium energy of this trajectory. Presented in figures 3.9(b)-(e) are four different points along the trajectory. For each point the circle centered at x_o, y_o tangent to M with radius $\sqrt{E_{eq}}$ is drawn, giving the equilibrium state and energy. As we move along the vertical trajectory, the radius of the tangent circle is first decreasing and then increasing, resulting in a energy landscape that we recognize as corresponding to regime (*i*), Section 3.2. Moreover, the equilibrium state of the system, the point (gray diamond) where the energy circle and the M curve meet, smoothly travels along the M curve.

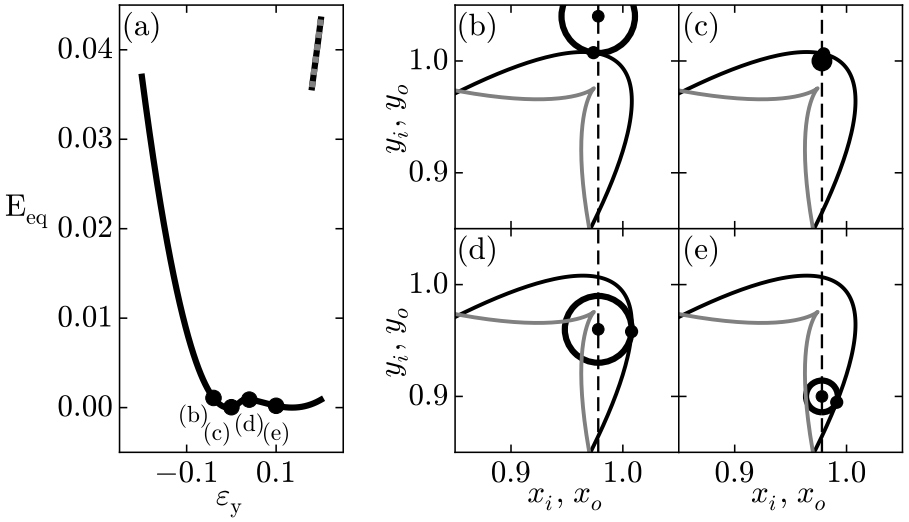

FIGURE 3.10: (a) Equilibrium energy of the vertical trajectory for a biholar mechanism with $\chi = 0.3$ and $x_o = 0.978$ ($\varepsilon = 0.0220$), which we associate with regime (*ii*). (b)-(e) Four different points at the trajectory with their corresponding equilibrium energy circles that are tangential to M. The equilibrium state $(x_o(\theta), y_o(\theta))$ is the point where the energy circle meets the M-curve (gray diamond).

Regime (ii) The value of x_o is chosen such that the trajectory is inside the M-curve but outside the evolute Σ, Fig. 3.10. As the line is outside Σ, only one equilibrium is present for each point on the trajectory. Moreover, as the trajectory crosses the M-curve twice, the radius of the tangential energy circle is first decreasing to zero (b)-(c) as it crosses the M-curve, then increasing (c)-(d) and decreasing again (e) as it crosses the M-curve for the second time. We recognize the corresponding equilibrium energy curve along this trajectory as fitting to regime (*ii*). Notice that the equilibrium state, indicated by the gray diamond, first stays roughly at the same location (b)-(c) on M and then rapidly, after the trajectory has crossed the M-curve for the first time, rapidly co moves along M. For lower values of y_o, higher values of ε_y, the trajectory will cross the M-curve, leading to two new energy equilibria, emerging from a saddle-note bifurcation, which are visible for high values of ε_y and E_{eq} in Fig. 3.10.

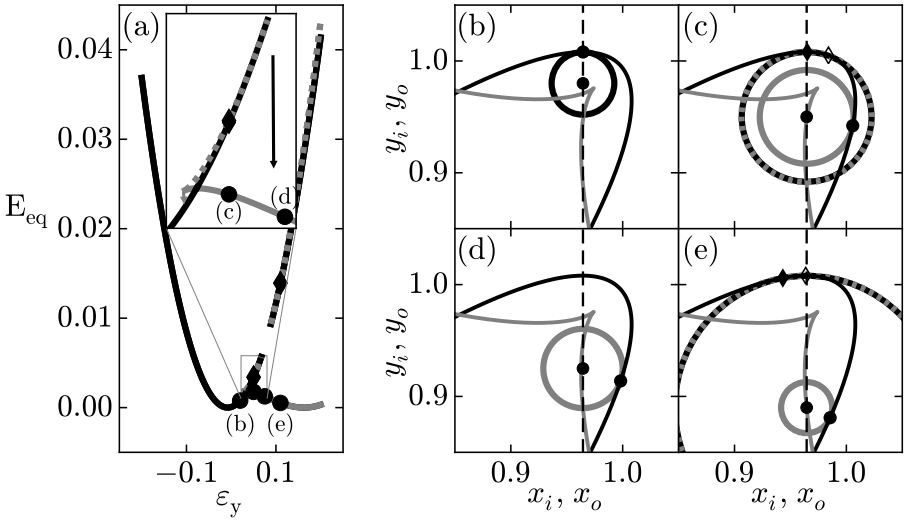

FIGURE 3.11: (a) Equilibrium energy of the vertical trajectory for a biholar mechanism with $\chi = 0.3$ and $x_o = 0.9665$ ($\varepsilon_x = 0.0335$), which we associate with regime (*iii*).(b)-(e) Four different points at the trajectory with their corresponding equilibrium energy circles that are tangential to M. The equilibrium states $(x_o(\theta), y_o(\theta))$ are the points where the energy circles meets the M-curve. (c) For points inside Σ, three equilibria are present. Black points correspond to a global minimum, black diamond to a local minimum, open black diamond to a local maximum. The colors of the energy circles match the colors for the different energy branches in figure (a). Dashed lines represent local maxima, full lines local minima, the coloring scheme matches that of Fig. 3.5.

Regime (iii) In Fig. 3.11, the value of x_o is chosen such that the trajectory crosses the M-curve once and the evolute Σ three times. Each crossing of the trajectory with the evolute is associated with the appearance or disappearance of a pair of local minima and maxima, i.e. saddle-node bifurcations. In Fig. 3.11(b) we show one circle with radius $\sqrt{E_{eq}}$ that is tangential to M, corresponding to small vertical compression. For larger compressions, (x_o, y_o) crosses the evolute and is now to the left of Σ, there are three circles that are tangent to M centered at (x_o, y_o), as shown in Fig. 3.11(c) (note that two of these are nearly identical). The tangent points correspond to the three equilibrium states of the mechanism, and are indicated by a black dot (global minimum), black diamond (local minimum)

and an open diamond (local maximum). The open diamond represents an unstable state. As indicated in Fig. 3.11(a), going from state (b)-(c), the system first follows a global minimum (black dot), which becomes a local minimum (black diamond) in figure 3.11(c), as a pair of local maxima and minima have appeared with a lower minimum energy. If (x_o, y_o) crosses the evolute again (Fig. 3.11(d)), a pair of energy minima and maxima annihilate in a reverse saddle-node bifurcation, and we are left with a single stable equilibrium state. This state is not smoothly connected to the stable state in Fig. 3.11(b) and (c), an the mechanism thus discontinuously jumps from the black branch to the gray branch (Fig. 3.11(a)). As (x_o, y_o) crosses Σ for the third time, and now is again inside the evolute (Fig. 3.11(e)), a forward saddle-node bifurcation occurs, leading to a pair of local maxima and minima (dotted gray and black lines in Fig. 3.11(a)), represented by dotted gray and black circles in Fig. 3.11(e). The preferred state of the system is still represented by the black dot on the M-curve as this is the minimum energy state and comoves along M by further increasing y_o.

Regime (iv) Finally, we increase the value of x_o such that the trajectory crosses both the evolute and M-curve once. In Figs. 3.12(b)-(c), (x_o, y_o) is outside the evolute, hence there is one (black) circle tangent to M centered at (x_o, y_o), corresponding to a single equilibrium state of the system (black dot). In Fig. 3.12(d), (x_o, y_o) is precisely at the evolute, resulting in two circles that are tangent to M corresponding to two equilibrium states of the mechanism, of which one is the minimum energy equilibrium state (black circle) and the other corresponds a local minimum *and* maximum (flat region in the $E(\theta)$-curve) that, as y_o is decreased furthermore, will segregate into two separate equilibrium states.
As y_o is decreased further, (x_o, y_o) crosses the evolute, and three lines tangent to M intersecting (x_o, y_o) can be drawn. Note that the state describing the system (black diamond) is not the minimum equilibrium energy state anymore, so that the mechanism is trapped in a local minimum. Moreover, as shown in Figs. 3.12(b)-(e), in contrast to the other three regimes, the marker describing the state of the system has moved towards higher values of θ (counter clockwise) on the M-curve when y_o is lowered.

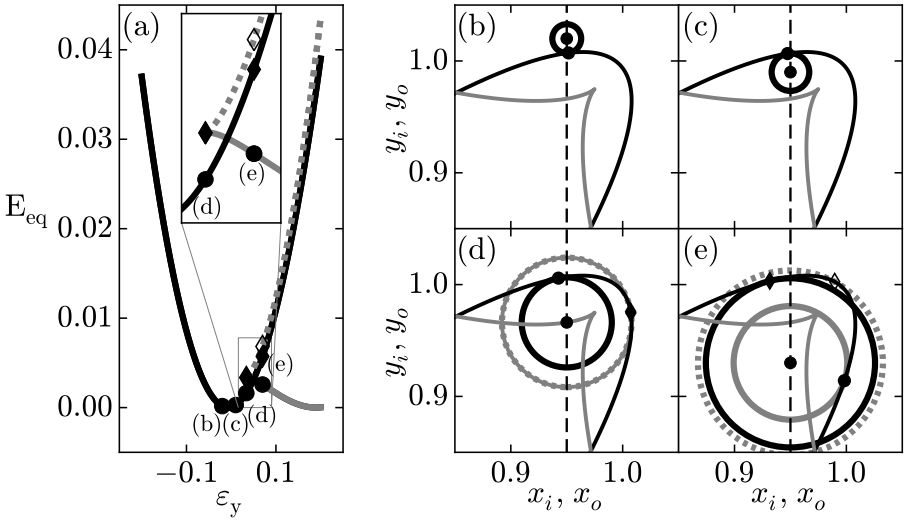

FIGURE 3.12: (a) Equilibrium energy of the vertical trajectory for a biholar mechanism with $\chi = 0.3$ and $x_o = 0.9500$ ($\varepsilon_x = 0.0500$), which we associate with regime (*iv*). (b)-(e) Four different points at the trajectory with their corresponding equilibrium energy circles that are tangent to M. (d) Precisely at Σ, two equilibria are present, of which one corresponds to a flat region in $E(\theta)$. Black points correspond to a global minimum, black diamondto a local minimum, open black diamond to a local maximum. The (dashed and full) colors of the energy circles match the colors for the different energy branches in figure (a), that matches the different bifurcation paths presented in Fig. 3.5.

Returning to Fig. 3.8, we can now summarize all our findings with a clear geometric interpretation of the three transitions. Curve A is tangent to M, so that here the energy is purely quartic in y_o, and $\partial_y F_y = 0$. Curve A thus separates *(i)* monotonic force curves at larger x_0 from *(ii)* non-monotonic force curves for smaller x_0. Curve B intersects the cusp of Σ, leading to a pair of saddle-node bifurcations which become separated for smaller x_o, and thus spawn a hysteresis loop. Curve B thus separates case *(ii)* and *(iii)*. Finally, curve C is tangent to Σ, which corresponds to a transcritical bifurcation where two solutions cross and exchange stability. As a result, for smaller x_o, the differently polarized branches decouple (Fig. 3.12). Curve C thus separates *(iii)* and *(iv)*. For movies illustrating the geometrical construction for cases *(i)-(iv)* as well as cases *A-C*, see Supplemental Information of [57].

3.4 Conclusions

We have demonstrated that the pattern transformations observed in a biholar sample can be mapped onto a single-degree-of-freedom mechanism consisting of rectangles connected by hinges at their corners. The state of this mechanism is described by a single parameter, θ.
In section 3.2 we have introduced the *soft mechanism*, a rigid mechanism coupled through a set of linear springs to the outside walls of a surrounding box, modeling the lateral and uniaxial confinement. The soft mechanism describes the mechanics of a laterally confined biholar sample under uniaxial loading well and gives insight in the different bifurcation scenarios leading to the four different mechanical regimes observed.
Additionally, by plotting the M-curve, which describes the state of the mechanism, the various transitions between the four regimes can also be explained by crossings of the experimental path, visible as vertical lines in this representation, with the M-curve and its evolute Σ. Each time the experimental path crosses the M-curve, there is a zero energy equilibrium state, while each time the experimental curve crosses the evolute, a saddle-node bifurcation occurs.
This geometrical interpretation suggests how to rationally design mechanical metamaterials with confinement controlled response: First, establish the required bifurcation scenario when ε_x is varied. Second, construct an evolute Σ that is consistent with the associated sequence of bifurcations. The M-curve can then explicitly be constructed as the *involute* of Σ [59]. Third, design a physical mechanism that possesses this M-curve; in principle any M-curve is encodable in a mechanism [60]. Finally, translate the rigid mechanism and hinges to a soft metamaterial with slender elements. Important work for the future is to explicitly demonstrate the feasibility of this design strategy [61].

APPENDIX A

DERIVATION OF THE MECHANICS OF THE BIHOLAR SOFT MECHANISM USING LAGRANGE MULTIPLIERS

Using Lagrange multipliers we can directly find an implicit relation between the force and deformation of the biholar soft mechanism. The Lagrangian is solely given by the potential energy:

$$\mathcal{L} = -2k_x\delta l_x^2 - 2k_y\delta l_y^2 \tag{A.1}$$

To find the equilibrium forces we minimize the Lagrangian subjected to two equations of constraints (Eq. 3.8 and Eq. 3.9):

$$\tilde{\mathcal{L}} = -2k_x\delta l_x^2 - 2k_y\delta l_y^2 + F_x(\delta l_x - x_o + x_i(\theta)) + F_y(\delta l_y - y_o + y_i(\theta)), \tag{A.2}$$

where F_x and F_y are the Lagrangian multipliers that represent the forces in the x- and y-direction. Minimizing $\tilde{\mathcal{L}}$ with respect to the variables δl_x, δl_y and θ results in the following set of equations:

$$\frac{\partial\tilde{\mathcal{L}}}{\partial\delta l_x} = -4k_x\delta l_x + F_x = 0 \tag{A.3}$$

$$\frac{\partial\tilde{\mathcal{L}}}{\partial\delta l_y} = -4k_y\delta l_y + F_y = 0 \tag{A.4}$$

$$\frac{\partial\tilde{\mathcal{L}}}{\partial\theta} = F_x\frac{\partial x_i(\theta)}{\partial\theta} + F_y\frac{\partial y_i(\theta)}{\partial\theta} = 0 \tag{A.5}$$

After substituting Eq. A.3 into Eq. A.5 we find two expressions for λ_y:

$$\lambda_y = -4k_y\delta l_y \tag{A.6}$$

$$\lambda_y = -4k_x\delta l_x \frac{\partial x_i(\theta)/\partial\theta}{\partial y_i(\theta)/\partial\theta} \tag{A.7}$$

We solve these two relations numerically to obtain a relation between force and deformation, $F(\varepsilon_y)$.

First the force $F(\theta)$ for every angle is calculated (Eq. A.7):

$$F(\theta) = -2k_x(x_o - x_i(\theta))\frac{b\cos(\theta) - a\sin(\theta)}{a\cos(\theta) - b\sin(\theta)} \tag{A.8}$$

Then we use Eq. A.6 to calculate δl_y for every angle θ:

$$\delta l_y = -F/4k_y \tag{A.9}$$

and finally we calculate the strain using:

$$\varepsilon_y = 1 - (y_i(\theta) - \delta l_y). \tag{A.10}$$